JOURNAL OF MATERIALS SCIENCE 30 (1995) 1818–1826

Damage evolution of angle-ply SCS-6/Ti composites under static and fatigue loading

P. C. WANG, S. M. JENG, H.-P. CHIU, J.-M. YANG
Department of Materials Science and Engineering, University of California, Los Angeles, Los Angeles, CA 90024-1595, USA

The effect of fibre orientation and laminate stacking sequence on the tensile and fatigue behaviour of SCS-6/Ti–15–3 composites were investigated. The laminates used in this study were: $(90)_6$, $(0/\pm 45)_s$, $(0/90)_s$, and $(90/\pm 45)_s$. The initiation and progression of microstructural damage at various stress levels was thoroughly characterized. It was found that fatigue life at high applied stresses were controlled by fibre fracture; progressive damage involving fibre fracture, interfacial debonding and matrix cracking became dominant at low applied stresses. Observation of the damage mechanisms in the angle-ply laminates under cyclic loading suggests that increasing the fibre–matrix bonding strength may improve the load carrying capability and fatigue life of laminates containing off-axis plies.

1. Introduction

Fibre-reinforced titanium matrix composites offer a promising potential for aerospace structural applications due to their high specific stiffness, strength and improved damage tolerance. Generally, unidirectionally reinforced composites exhibit the best properties along the longitudinal direction. However, a major drawback is that composites reinforced with unidirectional fibres usually display a large anisotropy in their inplane properties. As a result, unidirectionally reinforced titanium composites are only suitable for specific applications, such as hoop wound turbine engine rings [1]. The severe inplane anisotropy exhibited in the unidirectional composite can be eliminated by constructing various angle-ply laminates. Composites with a balance of mechanical properties will be used primarily in multi-axial loading applications such as hypersonic airframes. Obviously, before these materials can be safely implemented into critical structural components, a thorough understanding of their thermo–mechanical behaviour and damage evolution is required.

During past years, the mechanical behaviour and damage characteristics of unidirectional fibre reinforced titanium composites under various thermal and mechanical loadings have been investigated extensively [2–7]. Accordingly, approaches for life prediction for these materials in a complex thermo–mechanical environment are being developed. However, damage evolution in the multilayer angle-ply laminates is not well understood. This work was conducted to document the effect of fibre orientation on initiation and progression of microstructural damage in several angle-plyfibre reinforced titanium composites under static tensile and tension–tension cyclic fatigue loading.

2. Experimental procedure

The SCS-6/Ti–15 at % V–3 at % Cr–3 at % Al–3 at % Sn (Ti–15–3) composites were fabricated by Textron Specialty Materials (Lowell, MA) using a diffusion bonding technique. The reinforcing SCS-6 fibre is a continuous silicon carbide fibre with diameter of 140 μm and a carbon core. The fibre has a 3 mm carbon-rich coating, which is used to protect the fibre from strength degradation during composite processing. The composites used in this study were $(0/\pm 45)_s$, $(0/90)_s$, and $(90/\pm 45)_s$ laminates. The fibre volume fraction of each laminate was approximately 34%. A $(90)_6$ laminate was also used for comparison. The specimens for both tensile and fatigue tests had dimensions of 76.2 × 5.46 mm. Titanium alloy end tabs were epoxy bonded to both ends of the specimens to facilitate gripping during loading.

Tensile testing was conducted at room temperature on a screw driven Instron testing machine operating at a crosshead speed of 0.5 mm min^{-1}. Tensile strain was measured by epoxy bonding a thin foil electrical resistance strain gauge on one face of each specimen. In order to understand the damage development in the composites during the tensile testing, *in situ* replica and metallographic techniques were used. All specimens were pulled to failure. Fatigue tests were also performed at room temperature on a servo hydraulic Instron testing system with a loading frequency of 10 Hz, and the stress ratio, R, of 0.1. Tests were run at various maximum stress levels until the specimens failed.

The fracture surfaces under various testing conditions were examined by a scanning electron microscope to study their failure modes. Specimens were also mechanically polished to reveal the failure characteristics of each layer. Failure mechanisms were

0022–2461

then determined according to the information obtained.

3. Results and discussion

3.1. Tensile behaviour

Fig. 1 shows the stress versus strain curves of the $(0/\pm 45)_s$, $(90/\pm 45)_s$, and $(90)_6$ SCS-6/Ti–15–3 composites. The stress versus strain curve of a $(0)_6$ composite was also included for comparison. The initial elastic moduli, (E_i), ultimate tensile strength, UTS, and strain-to-failure derived from these stress–strain curves are given in Table 1. All the composites exhibited initial linear elastic stress–strain behaviour followed by a non-linear stress–strain response. The transition, "yielding", in the stress–strain curves occurred at different stress levels among these four laminates. For the $(0)_6$ and $(90)_4$ composites, the "yielding" occurred at 840 and 144 MPa, respectively. However, for the angle-ply $[(0/\pm 45)_s$ and $(90/\pm 45)_s]$ composites, "yielding" occurred at around 212 and 144 MPa, respectively. In order to understand the stress states in each laminate at the "yielding" point, the principal stresses (stresses parallel and perpendicular to the fibre direction) and shear stresses were calculated using lamination theory. The results are shown in Table II. Meanwhile, the radial stresses near the fibre–matrix interfacial region, calculated by using the four-zone model [8], are also listed in Table II. The results indicated that the shear stresses along the fibre–matrix interface in 45° fibres [62.4 and 79.8 MPa for $(90/\pm 45)_s$ and $(0/\pm 45)_s$ composites, respectively] were all lower than the interfacial shear strength (123 MPa) of the SCS-6/Ti–15–3 composite. This implies that "yielding" in angle-ply laminates is caused by opening of the fibre–matrix interface instead of interfacial shear debonding, which is quite different from the "yielding" mechanism of unidirectional composites (plastic deformation of the matrix) [9].

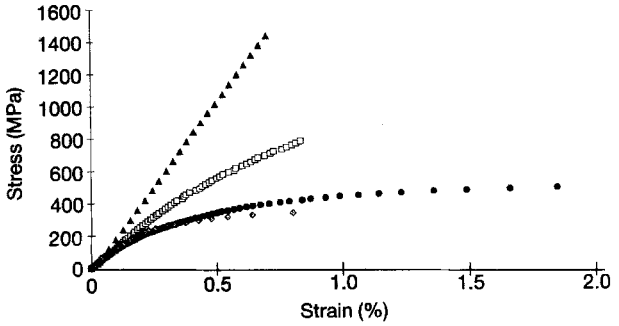

Figure 1 Stress versus strain curves of various SCS-6/Ti–15–3 laminates: ▲ $(O)_6$, □ $(0/\pm 45)_s$, ● $(90/\pm 45)_s$ ◈ $(90)_4$.

TABLE I Stress versus strain data of SCS-6/Ti–15–3 composites

	UTS (MPa)	Strain to failure (%)	Transition strength (MPa)	Initial elastic modulus (GPa)
$(0)_6$	1572	0.70	840	210
$(0/\pm 45)_s$	779	0.88	212	154
$(90/\pm 45)_s$	498	1.73	144	131
$(90)_4$	332	0.80	144	124

TABLE II Stresses in each lamina of the angle-ply composites

Stress (MPa)	$(90/\pm 45)_s$[a]		$(0/\pm 45)_s$[b]	
	(90)	(45)	(0)	(45)
σ_{11}[c]	134.4	73.5	272.5	121.1
σ_{22}[d]	−15.1	102.4	−10.4	87.4
τ_{12}[e]	0.0	62.4	0.0	79.8
σ_r[f]	140.5	106.5	−134.5	90.4

[a] The nominal stress is 144 MPa.
[b] The nominal stress is 212 MPa.
[c] σ_{11}, principal stress in the direction parallel to the fibre axis.
[d] σ_{22}, principal stress in the direction perpendicular to the fibre axis.
[e] τ_{12}, shear stress in the fibre–matrix interface.
[f] σ_r, radial stress in the fibre–matrix interface.

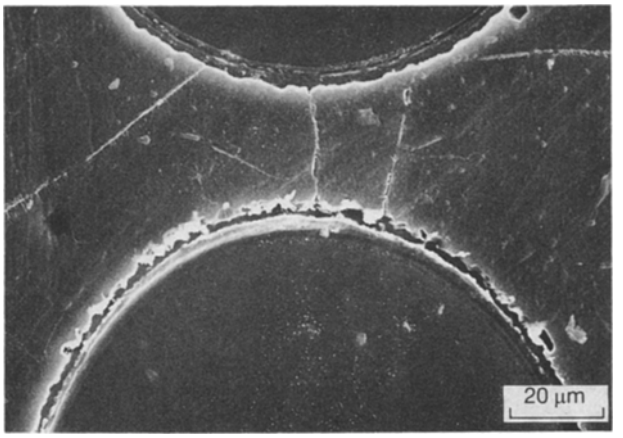

Figure 2 Interfacial fibre–matrix debonding occurs in the ± 45° layer of a $(0/\pm 45)_s$ laminate stressed around the "yielding" point (*in situ* replication image).

An *in situ* replication image for the $(0/\pm 45)_s$ composite loaded right above the "yield" stress is shown in Fig. 2. It clearly shows interfacial debonding in the ± 45° layers. Metallographic inspection of the 0° layer revealed that multiple fibre fracture without matrix cracking occurred throughout the whole gauge length (Fig. 3a). Closer examination indicated that interfacial damage, including multiple fracture of the reaction zone, microyielding of the matrix and interfacial debonding, also occurred in the region near the fracture surface. Similar tensile damage has also been found in a unidirectional SCS-6/Ti–15–3 composite [4]. However, for the ± 45° layers, fibre fracture and extensive fibre–matrix interfacial damage were only found near the fracture surface and free edges of the specimens, as shown in Fig. 3b. Fibre breakage was not observed away from the fracture surface. Also, cracking of the reaction zone and matrix microyielding did not occur in the ± 45° plies. This is due to release of the stresses along the fibre direction by the interfacial debonding of the ± 45° fibres during the early stages of tensile loading. The fracture surface of the $(0/\pm 45)_s$ laminate exhibited brittle fracture behaviour without significant fibre pull-out, as shown in

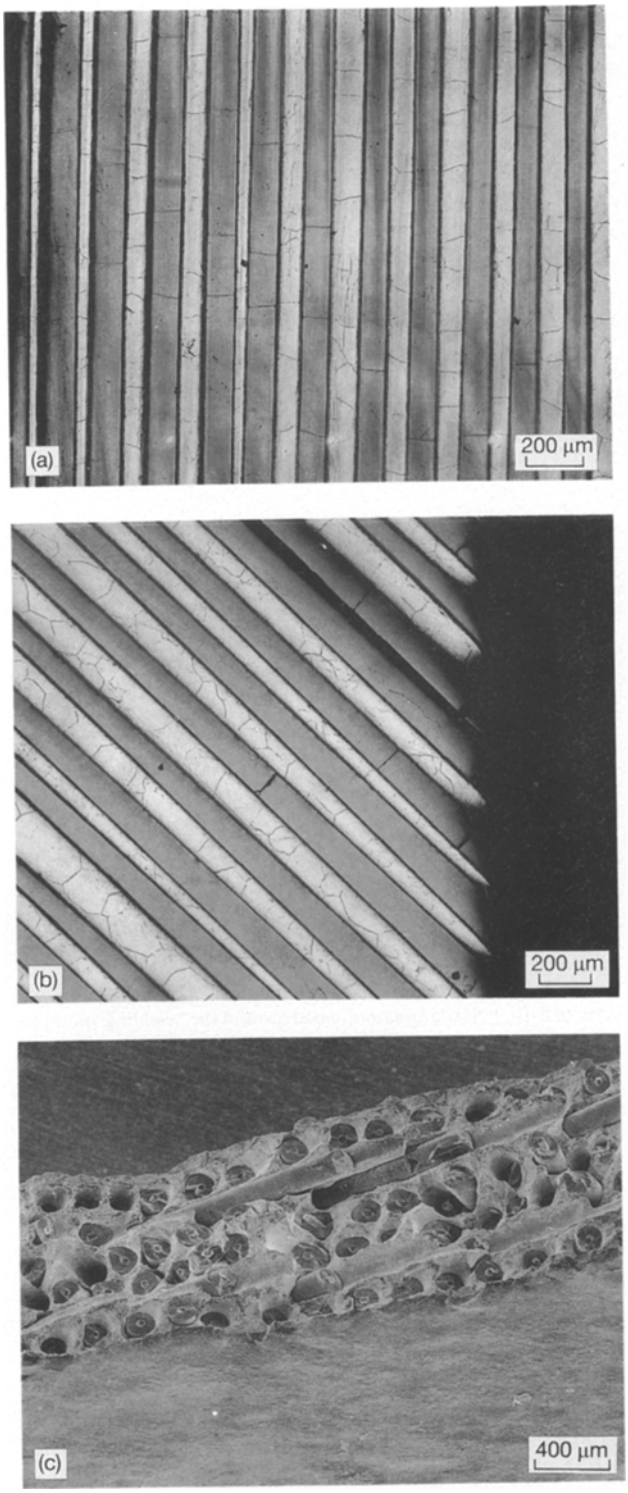

Figure 3 (a) Random multiple fibre breakage was observed in the 0° layer of the $(0/\pm 45)_s$ laminate, (b) fibre breakage was found near the free edge of the $\pm 45°$ layer of the $(0/\pm 45)_s$ laminate, (c) a typical tensile fracture surface of a $(0/\pm 45)_s$ laminate.

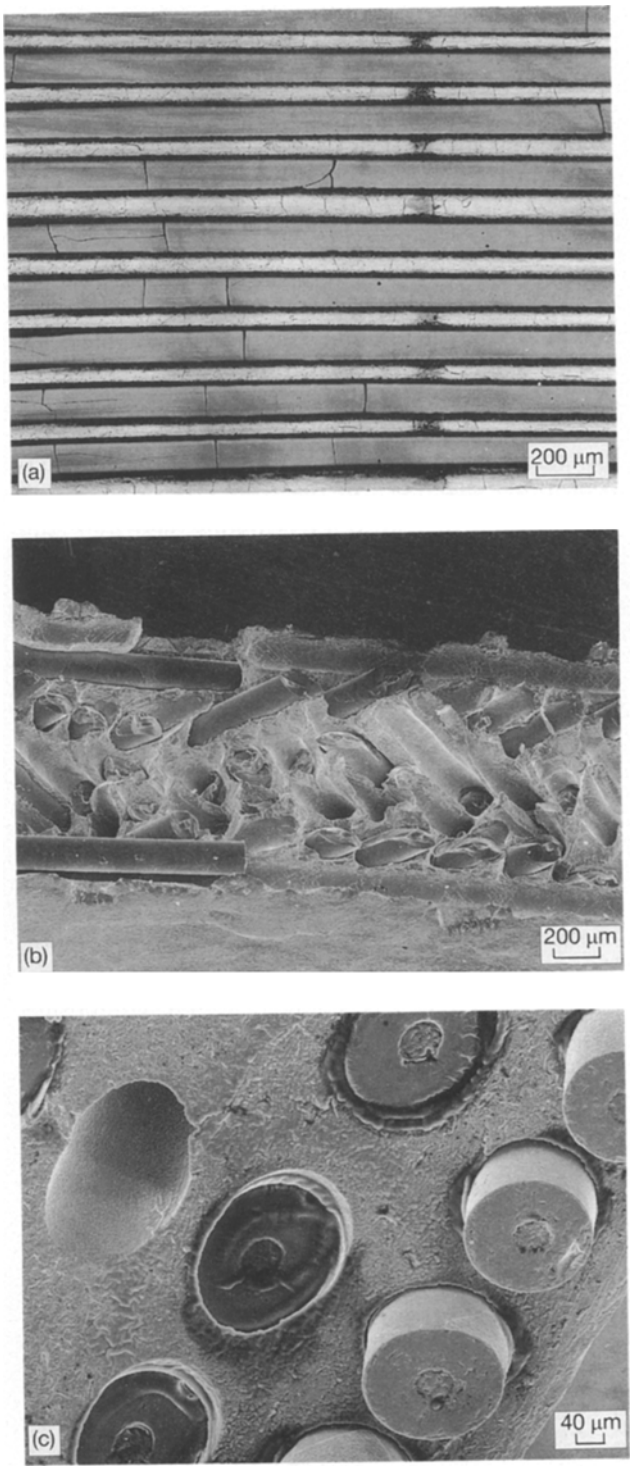

Figure 4 (a) Random fibre breakage was found in the 90° ply of a $(90/\pm 45)_s$ laminate, (b) typical tensile fracture surface of a $(90/\pm 45)_s$ laminate, (c) the edge of a post-fractured $(90/\pm 45)_s$ laminate shows protrusion of 90° fibres and intrusion of $\pm 45°$ fibres.

Fig. 3c. This implies that the final failure of the composite was controlled by the onset of fibre failure in the 0° layer.

Metallographic examination of the fractured $(90/\pm 45)_s$ specimens showed that extensive interfacial debonding occurred in both the 90° and $\pm 45°$ plies. Fibre fracture was observed near the fracture surface and free edges of the $\pm 45°$ plies. Random fibre breakage was also found throughout the 90° plies (Fig. 4a). The exact causes for breakage of the 90° fibres during the tensile test are still under investigation. However, a similar phenomenon was also observed in the SCS-6/Si_3N_4 composite under creep deformation [10]. No matrix cracking was found in either 90° or $\pm 45°$ plies. The typical tensile fracture surface of the $(90/\pm 45)_s$ laminate was perpendicular to the loading axis, as shown in Fig. 4b. The matrix exhibited typical ductile fracture patterns. This implies that the final failure of the composite was caused by the overload of the matrix alloy. Fig. 4c shows the edge of a post-fractured specimen. It clearly indicates the extensive protrusion of 90° fibres due to the difference of

the Poisson's ratios between the fibres and the matrix, and a slight intrusion of $\pm 45°$ fibres resulting from fibre rotation as the specimen elongated along the loading direction.

Based on the stress–strain behaviour and microstructural observations, the fracture process of the $(90/\pm 45)_s$ and $(0/\pm 45)_s$ laminates under tension is described as follows. For the $(0/\pm 45)_s$ laminate, when the applied nominal stress in the $\pm 45°$ plies reached the first knee (around 212 MPa), interfacial debonding (opening mode) initiated from free edges of the $\pm 45°$ plies, and propagated progressively along the fibre direction as the applied stress was increased. As a result, the load carrying capacity of the $\pm 45°$ layers gradually decreased. The resulting stiffness of the composite decreased as the stress was increased. The 0° layers thus became the principal load-carrying plies. Thereafter, the final failure was controlled by the 0° layers, and the failure mechanism was similar to that of $(0)_6$ described in [4].

When the $(90/\pm 45)_s$ specimen was subjected to tensile loading, interfacial debonding occurred in the 90° plies once the radial stress near fibre–matrix interface in the 90° plies reached the interfacial opening strength. Thereafter, the stiffness of the laminate decreased significantly. As the loading was further increased, interfacial debonding occurred at the $\pm 45°$ fibres when the nominal stress reached the interfacial opening strength. The debonding in $\pm 45°$ plies further reduced the stiffness of the laminate. Since extensive debonding occurred in both the 90° and $\pm 45°$ layers, the load was transferred to the matrix resulting in extensive plastic deformation in the matrix and a non-linear stress–strain response. Finally, overload of the matrix caused catastrophic failure of the laminate.

3.2. Low cycle fatigue behaviour

Fig. 5 shows the maximum cyclic stress versus fatigue life curves of the $(0/\pm 45)_s$, $(0/90)_s$ and $(90/\pm 45)_s$ composites. Also, the fatigue life of the $(0)_6$ composite was included for comparison [5]. It was noted that the fatigue limit (10^6 cycles without failure) of the $(0/\pm 45)_s$ composite was only slightly lower than that of the unidirectional composite (414 versus 470 MPa). However, the fatigue limit of the $(0/\pm 45)_s$ was three times higher than that of $(90/\pm 45)_s$ 414 versus 138 MPa). In order to understand the fatigue damage mechanisms and life-controlling parameters, the fatigue life data for the $(0)_6$, $(0/\pm 45)_s$ and $(0/90)_s$ composites were also plotted as a function of the initial applied stress in the 0° fibre. The initial applied stresses in the 0° fibre were calculated using the initial composite strain times Young's modulus of the fibre. The resulting fatigue life shown in Fig. 6 indicates that all composites exhibited a linear relationship between the initial stresses and fatigue life in the range of 3×10^3–2×10^5 cycles. This is quite different from the results obtained by Johnson [11], who showed that the fatigue lives of the $(0)_8$, $((0)_2/\pm 45)_s$, $(0/\pm 45/90)_s$, and $(0/90)_{2s}$ fit into a narrow band when fatigued below 5×10^4 cycles. The results shown in Fig. 6 suggest that fatigue damage of the unidirectional composite was more sensitive to the applied stresses than that of the angle-ply composites. This may be due to differences in the crack initiation and propagation mechanisms of these composites. As in the unidirectional composite, dominant fatigue damage modes in the angle-ply composites can also be classified into two regions: fibre breakage dominated and progressive damage dominated regions. The detailed microstructural damage characteristics in each region of these composites are described in the following sections.

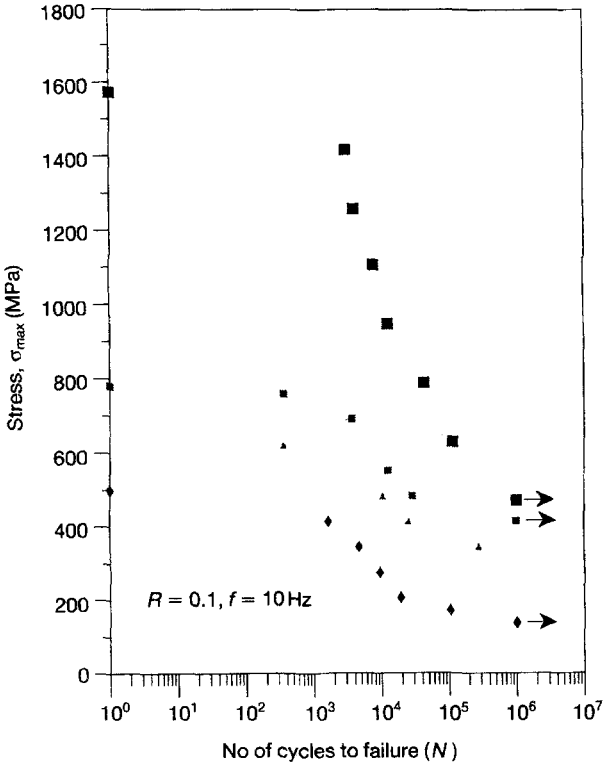

Figure 5 S–N curves of various SCS-6/Ti–15–3 laminates: ■ $(0)_6$, ■ $(0/\pm 45)_s$, ◆ $(90/\pm 45)_s$, ▲ $(0/90)_s$.

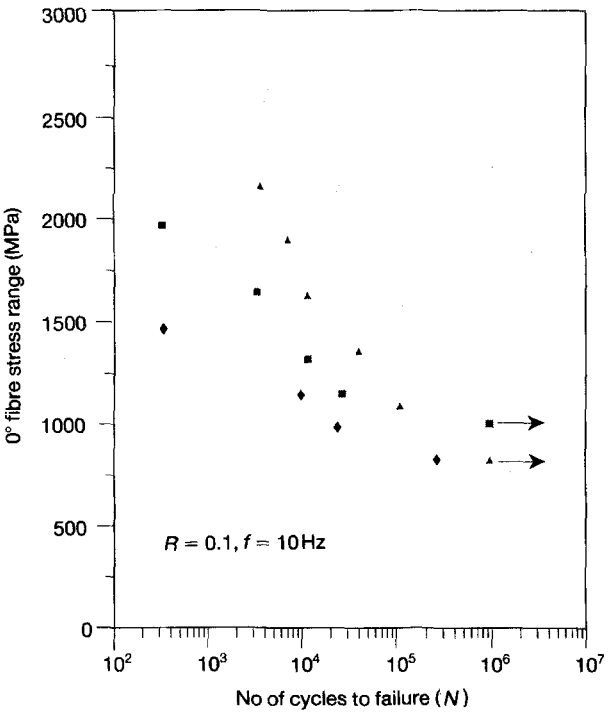

Figure 6 Cyclic stress range in the 0° fibre versus number of cycles to laminate failure: ▲ $(0)_6$, ■ $(0/\pm 45)_s$, ◆ $(0/90)_s$.

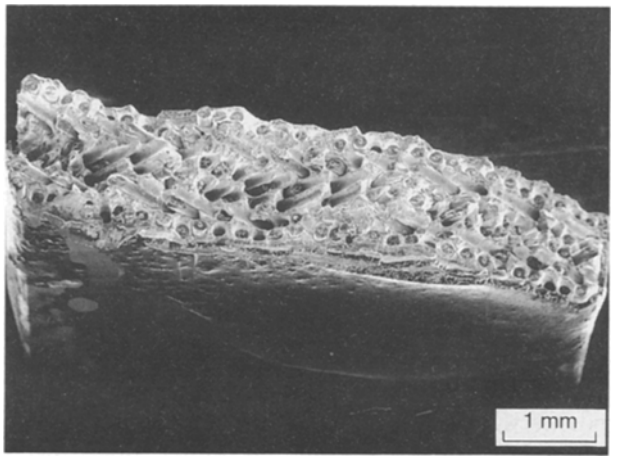

Figure 7 A typical fatigue fracture surface of a $(0/\pm 45)_s$ laminate that failed at high applied stress level.

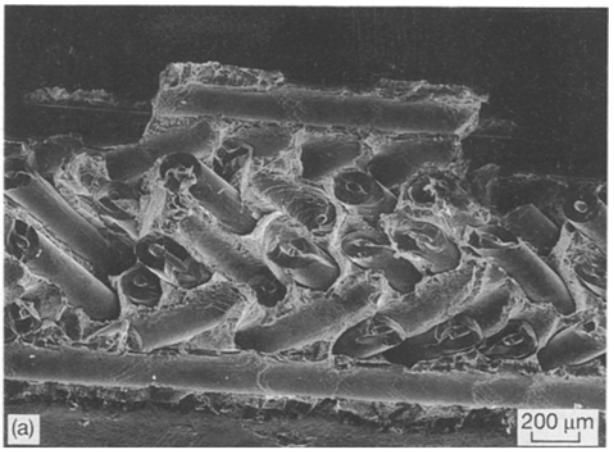

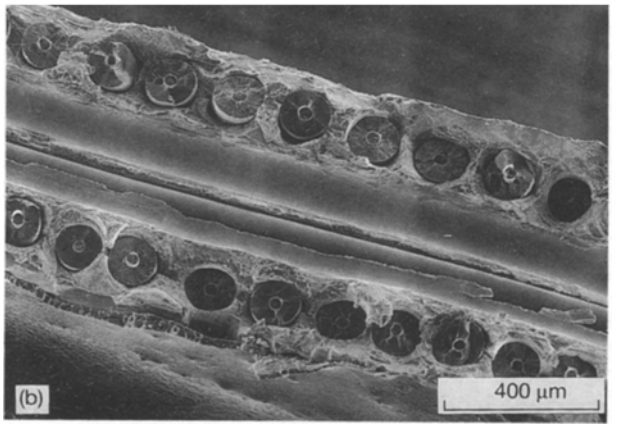

Figure 8 A typical fatigue fracture surface of (a) a $(90/\pm 45)_s$ and (b) a $(0/90)_s$ laminate that failed at high applied stress levels.

3.2.1. Fibre breakage dominated region

The fatigue life in this stress region was less than 3×10^3 cycles as shown in Fig. 6. A typical fracture surface of a $(0/\pm 45)_s$ laminate failed in this stress range is shown in Fig. 7. The matrix exhibited a typical tensile overload fracture pattern, and very limited fatigue striations were found near the fibre–matrix interface. Metallographic inspection of the post-fatigued specimens revealed that random multiple fibre fracture, microyielding of the matrix near the interface, and minimal matrix cracking occurred in the 0° layer. Meanwhile, for the $\pm 45°$ plies, most of the fibres away from the fracture surface remained intact, and the matrix was free of microyielding and cracking. Also, fibre–matrix debonding was limited to the vicinity of the fracture surface. These failure characteristics were similar to that for static tensile failure as shown in Fig. 3c.

For the $(90/\pm 45)_s$ and $(0/90)_s$ laminates, the fracture surfaces were very flat and perpendicular to the loading direction (Fig. 8a and b). Scanning electron microscope (SEM) observation indicated that fatigue striations were restricted to the regions near the fibre–matrix interface of the 90° layers. Also, no evidence of matrix cracking, fibre breakage, or interfacial debonding was found in the 0° or $\pm 45°$ and 90° plies away from the fracture surface.

Based upon the above observations, the failure processes of these three laminates in this stress range can be described as follows. Upon loading, interfacial debonding in the off-axis ($\pm 45°$) or transverse (90°) layers occurs after the first few fatigue cycles. The loss of load carrying capability in the off-axis or transverse layers could lead to high stresses in the 0° layers. As a result, the final failure of the composite is controlled by fracture of the 0° fibres.

3.2.2. Progressive damage region

The fatigue life in this stress range is higher than 3×10^3 cycles as shown in Fig. 6. A typical fracture surface of a $(0/\pm 45)_s$ composite that tested at this range is shown in Fig. 9a. The fracture surface was serrated without significant fibre pull-out or exposure of the off-axis fibres. Close examination of the matrix in the composite revealed two major failure characteristics: fatigue striation patterns and microvoid coalescence (Fig. 9b). The fatigue striation patterns were found around the interfacial region at the $\pm 45°$ fibres and among these regions was the typical microvoid coalescence failure mode. Meanwhile, the fatigue striation region increased as the maximum stresses decreased. Metallographic examination of the cross-section (perpendicular to the loading direction) of the specimen tested at high stress level ($\sigma_{max} = 690$ MPa) showed that matrix cracking was prone to initiate from the interfacial region of the $\pm 45°$ layers and radially extended into neighbouring layers, as shown in Fig. 10a. However, when the applied stress was reduced ($\sigma_{max} = 483$ MPa), matrix cracking that initiated from the fibre–matrix interfacial region of the 0° layer was also observed (Fig. 10b). As a result, the matrix cracking density increased significantly.

Fig. 11 a and b are typical polished surfaces of the 0 and $\pm 45°$ layers, respectively. Significant matrix cracking was observed in both layers as expected. The matrix cracking tended to grow perpendicular to the fibre direction in the $\pm 45°$ layers. However, in the 0° layer, matrix cracks were tilted 45° to the fibre direction. By overlapping these two micrographs, it was found that the matrix cracks in these two layers were along the same direction. This further confirms that matrix cracks initiated from the $\pm 45°$ layers and subsequently propagated into the 0° layers. Furthermore,

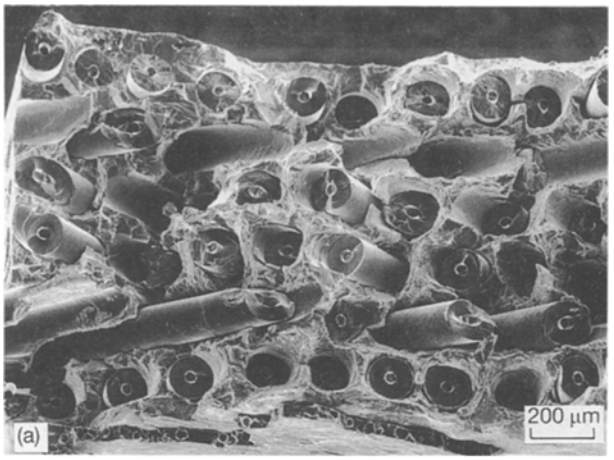

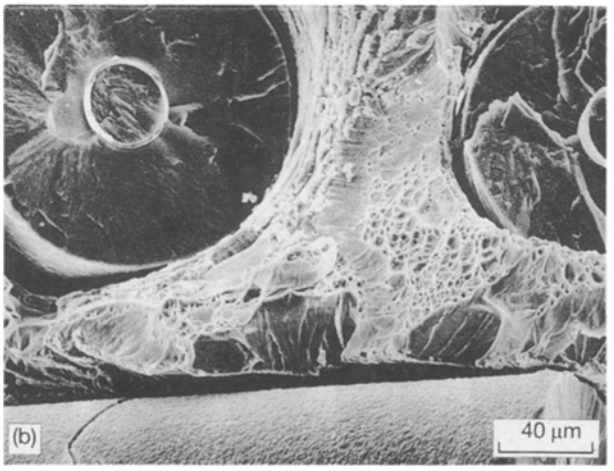

Figure 9 (a) A typical progressive fatigue fracture surface of a $(0/45)_s$ laminate ($\sigma_{max} = 690$ MPa), and (b) a mixture of fatigue striations and microvoid coalescence.

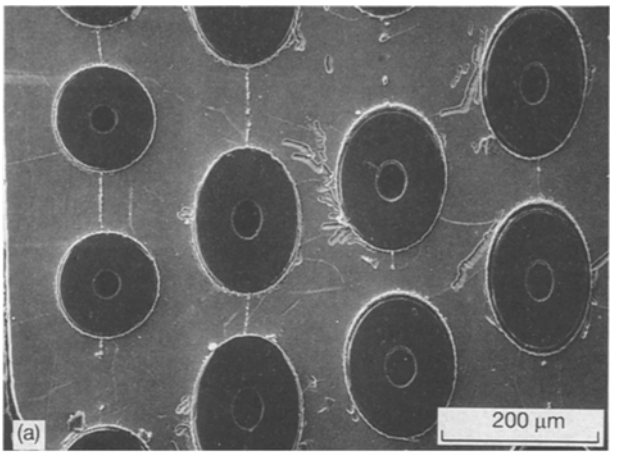

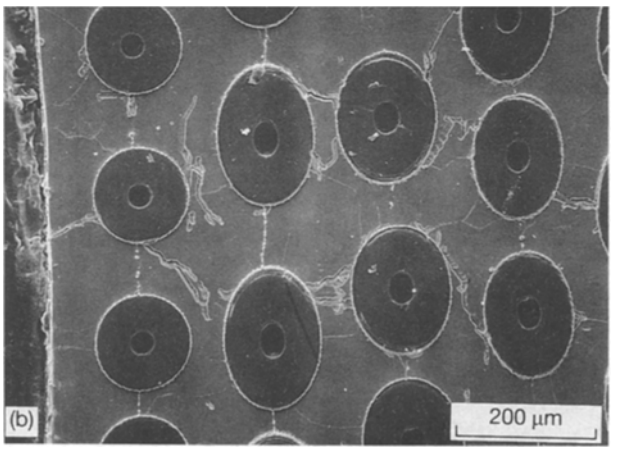

Figure 10 The matrix fatigue cracking pattern in the cross-section of a $(0/\pm 45)_s$ laminate where the cyclic loading axis is perpendicular to the surface of the photograph. (a) $\sigma_{max} = 690$ MPa, (b) $\sigma_{max} = 483$ MPa.

random fibre breakage in the 0° layer was observed across the whole specimen. However, in the $\pm 45°$ layers, fibres were unbroken and bridged the cracked matrix. Fig. 12a, b further illustrates the origin of fatigue crack initiation and growth near the fibre–matrix interfacial region in the 45° layer. Fig. 12a clearly shows that a long interfacial debonding crack was formed between the reaction and carbon coating layers. Meanwhile, a small crack initiated at the reaction layer, and subsequently propagated into the matrix, as shown in Fig. 12b. The above microstructural observation clearly indicates that the interfacial debonding along the 45° fibres occurred at the first few cycles. This can further be confirmed by the static tensile test in which interfacial debonding occurred at applied stresses above 414 MPa. Upon further cyclic loading, the interfacial reaction layer at the $\pm 45°$ layers served as crack initiation sites. As cracks from the $\pm 45°$ layers further propagated, more and more load transferred to the 0° layers. Finally, matrix cracks in the 0° plies initiated.

For the $(0/90)_s$ and $(90/\pm 45)_s$ laminates, the fracture surface showed that fatigue striations were the major damage mode of the matrix in the 90° layers. However, the matrix in the 0 or $\pm 45°$ layers exhibited a mixture of fatigue striations and ductile dimple failure morphology. When examining the specimen edges, it showed that matrix cracks extending from the interfacial region of the 90° layers was the primary damage mechanism for both composites. However, as the applied stresses were further decreased, matrix cracks initiating from the interfacial reaction layers in the 0 and $\pm 45°$ layers for the $(0/90)_s$ and $(90/\pm 45)_s$ laminates were also observed as shown in Fig. 13a, b, respectively. Fig. 14a–c are typical polished surfaces for the 0 and $\pm 45°$ layers of $(0/90)_s$ and $(90/\pm 45)_s$, respectively. Instead of extensive matrix microcracking as observed in the $(0/\pm 45)_s$ laminate, only a few matrix cracks were observed in these layers. Random fibre fracture in the 0° layer occurred in the $(0/90)_s$ laminate. Fibre breakage in the $\pm 45°$ layer also occurred around the matrix cracks at a high applied stress ($\sigma_{max} = 283$ MPa) as shown in Fig. 14b. However, fibres in the $\pm 45°$ layers remained unbroken and bridged the cracked matrix in the $(90/\pm 45)_s$ laminate when the applied stress was decreased ($\sigma_{max} = 138$ MPa) as shown in Fig. 14c. These results suggested that damage initiation and propagation at the 90° layers dominated the fatigue life of these two laminates.

From the above microstructural observations, it is evident that the fatigue damage is primarily initiated by interfacial opening of the $\pm 45°$ layers of $(0/\pm 45)_s$,

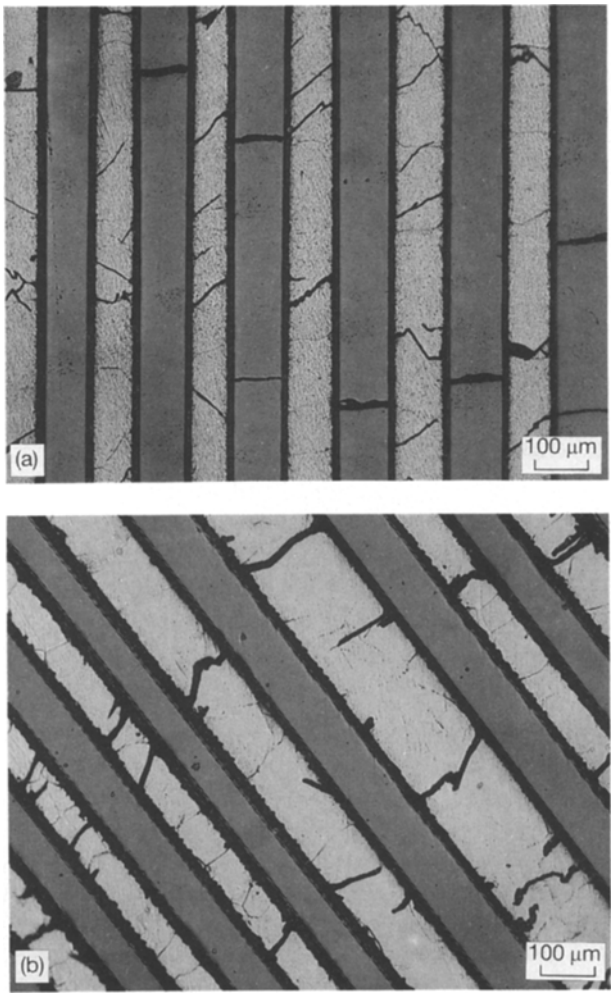

Figure 11 (a) Fibre breakage and matrix cracking pattern in the 0° layer of a $(0/\pm 45)_s$ laminate, and (b) matrix cracking pattern in the $\pm 45°$ layer of a $(0/\pm 45)_s$ laminate.

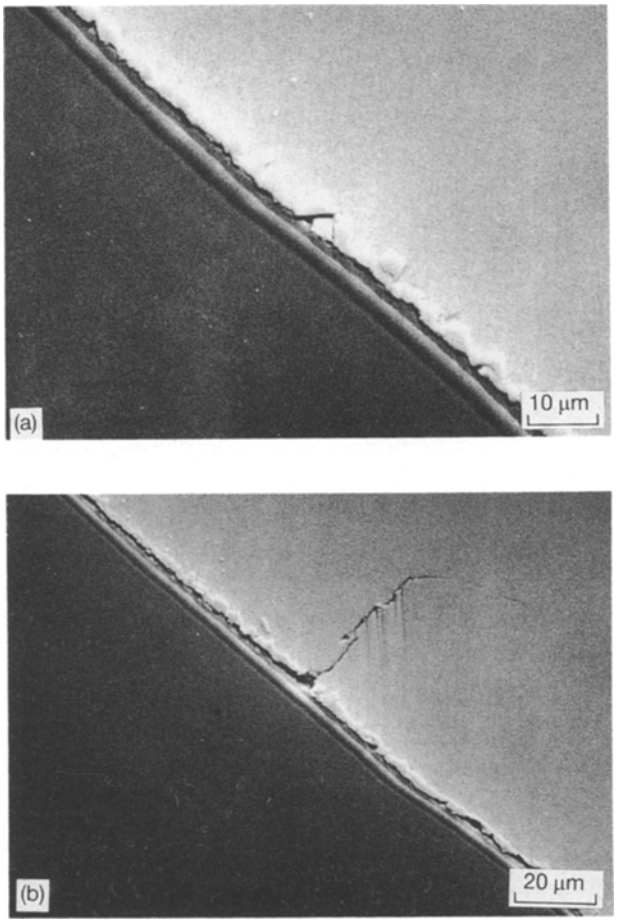

Figure 12 Fibre–matrix interfacial debonding associated with (a) the initiation of a matrix crack, and (b) a matrix crack.

and 90° layers in both $(0/90)_s$ and $(90/\pm 45)_s$ laminates. After initiation, the fatigue crack propagation in the laminates containing 90° layers occurred in a well defined manner. Several long cracks were found in the whole specimen and these cracks were constrained along the fibre–matrix interface of the 90° layers. However, in the $(0/\pm 45)_s$ laminate, most of the fatigue cracks tended to propagate perpendicular to the fibre direction in the $\pm 45°$ layers. Also, these cracks spread randomly across the whole specimen without any long cracks. This phenomena was also observed in the fatigue crack propagation behaviour of the notched $(0/\pm 45)_s$ composite [12]. During fatigue testing, a huge damage zone containing extensive matrix microcracks was formed in front of the primary crack. These cracks were initiated from the interfacial region in the $\pm 45°$ layers. Since the load released by the cracked matrix would gradually be transferred to the major load carrying fibres (0° fibres), fibre breakage could occur near the cracked matrix region.

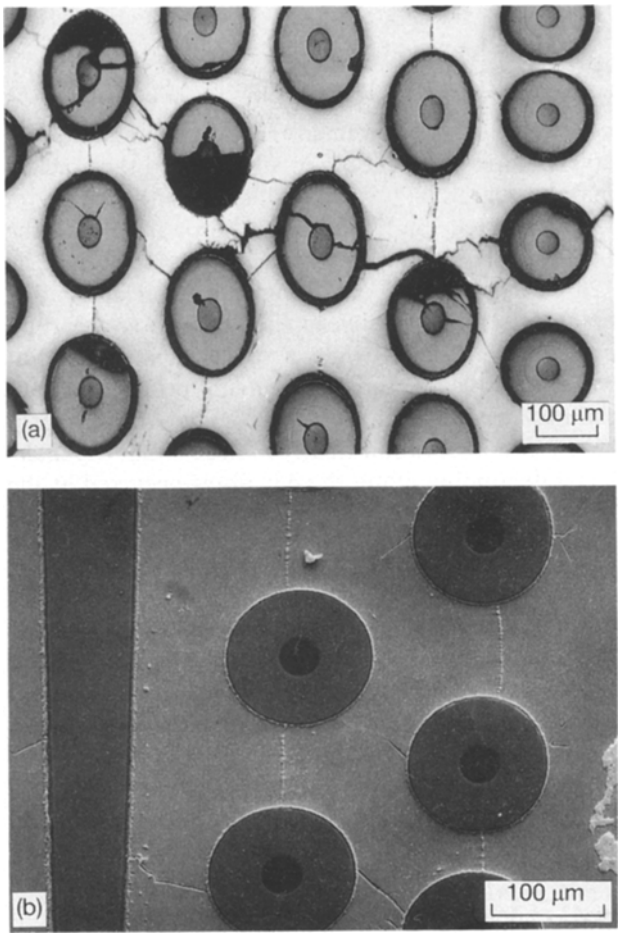

Figure 13 Matrix cracks developed in both (a) the ± 45 and 90° layers of the $(90/\pm 45)_s$ laminate, and (b) the 0 and 90° layers in the $(0/\pm 90)_s$ laminate.

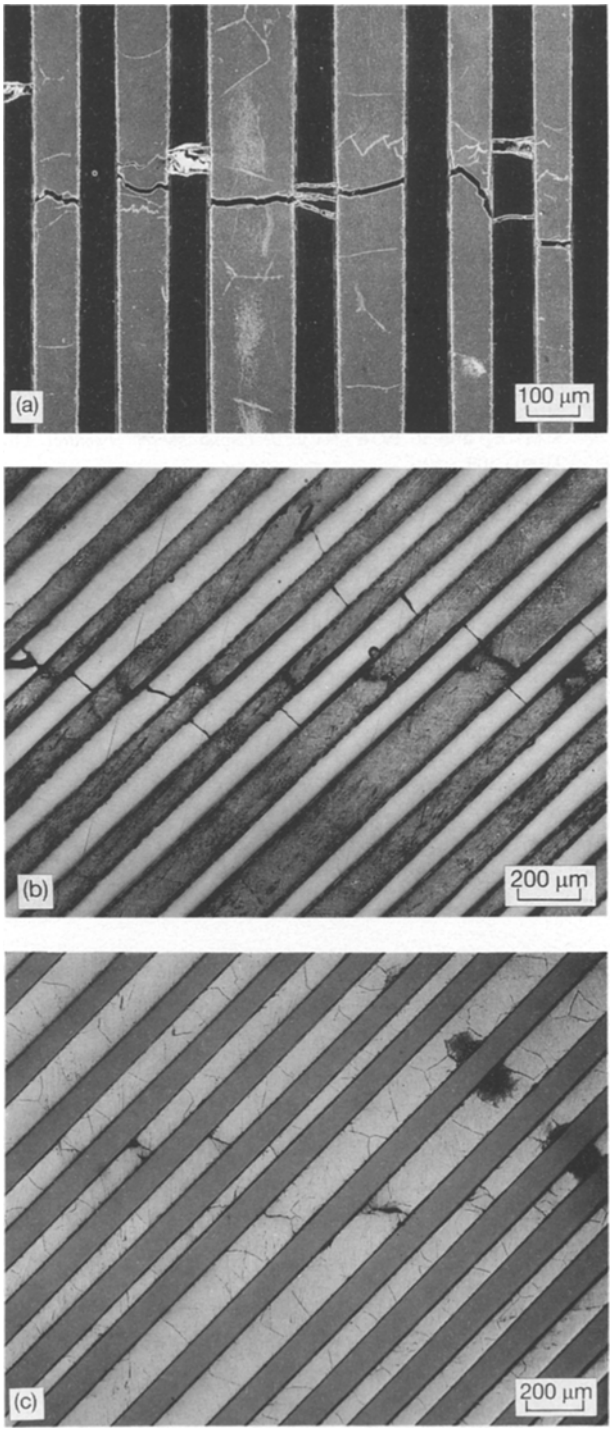

Figure 14 A continuous matrix crack (a) developed in the 0° ply of the $(0/90)_s$ laminate, and (b) associated with fibre breakage in the $\pm 45°$ layer of the $(90/\pm 45)_s$ laminate ($\sigma_{max} = 283$ MPa), (c) only a few matrix cracks developed in the $\pm 45°$ ply of the $(90/\pm 45)_s$ laminate, while the fibres in this ply remained unbroken ($\sigma_{max} = 138$ MPa).

However, due to extensive interfacial debonding of the off-axis layers, the fibres in these layers could survive during the fatigue loading. The final failure of the composites could be controlled by the critical amount of fibre breakage in the 0° or major load carrying layers.

As discussed in the unidirectional composite [5], the fatigue life in this region is controlled by the number of crack initiation sites and crack propagation rate. For the unidirectional composite, matrix cracks were initiated at surface defects (especially the damage from mechanical machining) and cracking of interfacial reaction layers. However, crack initiation in the angle-ply composite is controlled by the interfacial opening (mode I failure) of the off-axis layers. The stress levels required to initiate microscopic damage in the unidirectional and angle-ply laminates can be assessed by comparing the cracking strength and the interfacial opening strength of reaction layers in the SCS-6/Ti–15–3 composites. As discussed in the previous section, the applied nominal stresses required to cause interfacial opening were found to be 212 and 144 MPa for the $(0/\pm 45)_s$ and $(0/90)_s$, respectively. These are far weaker than the fracture strength of the reaction layer (551 MPa for the SCS-6/Ti–15–3 composite [4]). As a result, the fatigue damage initiation in the angle-ply composites could occur at a stress level much lower than that of the unidirectional composite. Furthermore, the applied stress needed to induce interfacial opening could decrease as the angle of the off-axis layers increases. This further suggests that these off-axis layers could become dominant damage sources in the angle-ply laminates. Regarding fatigue crack propagation, the life of a unidirectional composite is controlled by the unbroken fibre bridging effect in the wake of the matrix cracks. However, in the angle-ply composites, the volume fraction of the 0° fibres is definitely lower than that in the unidirectional composite. This indicates that fibre bridging could be less effective in reducing stress intensity at the crack tip. Also, significant multiplication (initiation and coalescence) of matrix microcracking in the angle-ply layer could also increase the damage accumulation (propagation) rate and reduce the load carrying capability of the laminate. Meanwhile, the stresses in the matrix are also higher than those in the unidirectional composite for the same applied stress. Furthermore, for the angle-ply laminates containing (90) layers, the weak interfacial opening strength generates a fast crack propagation path. A previous study on the fatigue crack propagation behaviour in notched composites also indicated that the angle-ply laminate exhibited lower transition stresses (K_{max}) between non-catastrophic to catastrophic failure than that of the unidirectional composite [12]. These results further confirmed that the unidirectional composite has better fatigue resistance than that of the angle-ply composites. Increasing the angle of the off-axis layers would further decrease fatigue life.

4. Conclusion

The damage initiation in the angle-ply composites under tensile static and cyclic loading is dominated by the interfacial opening strength. This implies that improvement of the interfacial opening strength is necessary for better tensile and fatigue properties of these composites. This is different from the case in the unidirectional composite, where the major issue is to control the thickness of the interfacial reaction layer, to prevent premature cracking of the

interfacial reaction layer and degradation of fibre strength.

Fatigue damage initiation and accumulation mechanisms of the angle-ply and cross-ply composites have been clearly identified. These are extensive interfacial debonding in off-axis layers, 0° fibre breakage, matrix cracking perpendicular to the 45° fibre, crack propagation along the fibre–matrix interface in 90° layers. These damage characteristics have different effects on the residual mechanical properties of the composite under fatigue loading. A systematic study on the effect of each damage mode on property degradation is necessary for developing life prediction methodology.

Acknowledgements

This work was partially supported by the Air Force Office of Scientific Research. Dr Walter Jones is the program monitor.

References

1. B. A. LERCH and J. F. SALTMAN, "Tensile Deformation Damage in SiC Reinforced Ti-15V-3Cr-3Al-3Sn," NASA TM-103620 (NASA Lewis Research Center, Cleveland, OH, 1991).
2. W. S. JOHNSON, S. J. LUBOWINSKI and A. L. HIGHSMIT, "Thermal and Mechanical Behaviour of Metal Matrix and Ceramic Matrix Composites", ASTM STP 1080, edit. by J. M. Kennedy, H. H. Moeller, and W. S. Johnson (American Society for Testing and Materials, Philadelphia, 1990) pp. 193–218.
3. T. P. GABB, J. GAYDA and R. A. MACKAY, J. Compos. Mater. **24** (1989) 667.
4. S. M. JENG, J.-M. YANG and C. J. YANG, Mater. Sci. Engng A **138** (1991) 169.
5. S. M. JENG, P. ALASSOEUR and J.-M. YANG, *ibid.* **148** (1991) 67.
6. B. S. MAJUMDAR and G. M. NEWAZ, "Composite Materials: Fatigue and Fracture" Vol. 3, ASTM STP 1110, Edt. by T. K. O'Brien (American Society for Testing and Materials, Philadelphia, 1991) pp. 732–752.
7. S.MALL and B. PORTNER, *J. Engng Mater. Technol.* **114** (1991) 409.
8. Y. MIKATA and M. TAYA, *J. Comp. Mat.* **19** (1985) 554.
9. B. S. MAJUMDAR and G. M. NEWAZ, "Inelastic Deformation of Metal Matrix Composites, Part I - Plasticity and Damage Mechanisms", NASA CR-189095 (NASA Lewis Research Center, Cleveland, OH, 1992).
10. J.-M. YANG and S. T. CHEN, Adv. Compos. Lett. **1** (1992) 27.
11. W. S. JOHNSON, in "Metal Matrix Composites: Testing, Analysis and Failure Modes", Edited by W. S. Johnson (American Society for Testing and Materials, Philadelphia, PA 1989) pp. 194–221.
12. T. H. BRUCE NGUYEN, S. M. JENG and J. M. YANG, *Mater. Sci. Engng* (1993).

Received 9 September 1993
and accepted 6 July 1994